

# Sound radiation from a line forced perforated elastic sandwich panel

I. David Abrahams

*Department of Mathematics, University of Manchester, Oxford Road, Manchester M13 9PL,  
United Kingdom*

(Received 16 April 1998; revised 31 October 1998; accepted 11 March 1999)

Composite barriers, consisting of thin plates separated by light matrix structures, are widely used for fuselage construction in the aircraft industry, and in partitions in the building trade. The acoustical properties of such materials can vary considerably by altering the interior geometry, and perforations can be added to one or both sides. With perforations the interior cavities can act as Helmholtz resonators, causing a substantial modification to the overall transmission and reflection properties of such barriers. Leppington [Proc. R. Soc. London, Ser. A **427**, 385–399 (1990)] devised an effective boundary condition for a perforated sandwich plate structure, valid in the limit of low frequency (acoustical waves long compared with the typical dimensions of the hole/cavity construction), and obtained transmission and reflection coefficients for infinite planar structures. This article investigates the radiation properties of perforated sandwich plates by examining a simple infinite one-dimensional model (employing Leppington's effective boundary condition) which is loaded by a line force or moment. The radiated far field, and unattenuated subsonic plate wave coefficients, are found explicitly, and are plotted over a range of frequencies for two physical configurations, namely an aluminum plate in water and in air. It is revealed that, unlike the usual thin plate equation, the model discussed herein has two bi-directional unattenuated plate waves, and for the structure in air the two waves are of similar magnitude over most frequencies. Surprisingly, these amplitudes are shown to become very large at a frequency below that of the structure's Helmholtz resonance frequency. Further, the field radiating into air is also significantly modified by the cavity/perforations well away from the Helmholtz frequency. © 1999 Acoustical Society of America. [S0001-4966(99)04006-0]

PACS numbers: 43.20.Fn, 43.30.Jx, 43.40.Dx, 43.40.Fz [CBB]

## INTRODUCTION

Sound transmission through panels has long been a subject of importance in a variety of applications, including room acoustics<sup>1</sup> and aeroacoustics. In the latter application, for instance in the fabrication of aircraft fuselages, the bodies are often of a sandwich construction composed of two thin-plates separated by stiffeners or ribs in between.<sup>2</sup> The transmission and reflection of sound waves through the sandwich structure is determined by the properties of the plates and the enveloping fluid. In aircraft, and in particular helicopter designs, it is usually the case that sound transmission is required to be minimized over a specific range of frequencies. Sound transmission can be ameliorated to some extent by adding perforations to one or both sides of the flexible structure.<sup>3,4</sup> Leppington<sup>5</sup> examined the simple but physically realistic model of a perforated sandwich panel; namely one constructed of a honeycomb cellular structure (usually made of thin foil or similar material) bounded by two planar thin elastic plates. Perforations were included on one side of the structure. Leppington's model can accommodate variations in size of the cavities, number of perforations as a fraction of the number of cavities, perforation hole size, etc. The only restriction on the model is that the wavelength of the acoustic waves is long compared with the length scales of the composite structure, i.e., cavity width and height, thickness of thin plates and perforation hole size. In this limit the sound field will experience the "averaged" effect of the

sandwich structure rather than scattering/radiation from the individual cells. Leppington exploited this fact to solve the transmission and reflection problem, of long waves incident on the sandwich structure, by the method of matched asymptotic expansions. He showed that the cavities with small holes behave as individual Helmholtz resonators which dramatically alter the pressure field on the perforated (upper) side of the plate near the resonance frequency. The upshot is that away from a resonance the barrier behaves as a single elastic plate (in the long wavelength limit), with fluid on both sides, but near the Helmholtz frequency the sound transmission is significantly reduced with almost all energy reflected. In the latter case it is as if there is no fluid above the barrier.

In his article, Leppington<sup>5</sup> concluded with the derivation of a new plate equation which included the effects of the cavities and perforations. This reproduced his results found by matching, and is a very useful approximate boundary condition that can be employed in more complicated model problems. In particular, it is important to understand how the sandwich panel scatters acoustic waves as well as its transmission and reflection properties. In the former case only can energy be fed into the flexural wave mode of the structure and this could have significant consequences on the sound field above and below the composite plate. Jones<sup>6</sup> discussed the canonical scattering problem of a semi-infinite sandwich panel attached to a rigid half-screen and irradiated by plane waves from below. Unfortunately, the semi-infinite geometry

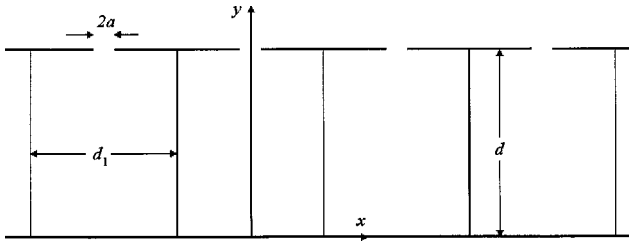


FIG. 1. The perforated plate construction.

adds significantly to the mathematical complexity, and the boundary value problem is reduced to a matrix Wiener-Hopf problem. Such equations cannot, in general, be solved exactly (see, for example, Ref. 7), although an approximate procedure has recently been presented by the author<sup>8</sup> which can be applied<sup>9</sup> to the class of matrices to which the one examined by Jones<sup>6</sup> belongs. However, Jones merely restricted attention to the case when the effect of the perforations almost vanished, and hence obtained a perturbation solution for which the standard scalar Wiener-Hopf technique is applicable. Jones did not obtain any numerical results.

On reexamining Jones' model problem using the method described in Ref. 9 by the author, and performing a numerical investigation over all values of the perforation parameter  $\tau$ , various results regarding the scattered field and traveling plate waves were deduced. These were sufficiently perplexing<sup>10</sup> to justify appraisal of a simpler radiation problem, which avoids the complexity of a Wiener-Hopf analysis. In particular, we demonstrate that Leppington's plate model<sup>5</sup> has two unattenuated wave modes for all nonzero values of the fluid/plate parameters. Apparently, this result has hitherto not been noticed by others. The problem to be discussed here consists of an infinite planar perforated elastic plate immersed above and below in a compressible stationary fluid. A time-harmonic line force provides the excitation and we seek the cylindrically radiating sound field plus the coupled surface wave terms. The paper is constructed as follows: in the following section the boundary value problem is posed, and in Sec. II the dispersion relation for unattenuated waves on the perforated plate is derived and then shown to have two real roots. In Sec. III the boundary value problem is solved by recourse to Fourier transforms, from which the radiated far-field and plate wave coefficients are deduced. In the final section we examine the behavior of these quantities for variations in the numerical values of parameters (consistent with physical models) and concluding remarks are offered.

## I. THE BOUNDARY VALUE PROBLEM

The boundary value problem is summarized in Fig. 1. It consists of a compressible, stationary fluid occupying the whole of space, outside of the plate, for which time-harmonic small disturbances are governed by

$$\frac{\partial^2 \phi}{\partial x^2} + \frac{\partial^2 \phi}{\partial y^2} + \frac{\partial^2 \phi}{\partial z^2} + \frac{\omega^2}{c_0^2} \phi = 0. \quad (1)$$

Here  $(x, y, z)$  are dimensional Cartesian coordinates,  $\phi(x, y, z, t)$  is the velocity potential of the acoustic perturba-

tion,  $\omega$  is the oscillation radian frequency, and  $c_0$  is the sound speed in the fluid at rest. The fluid pressure fluctuations,  $p$ , and the density fluctuations,  $\rho$ , are related to the potential via

$$p(x, y, z, t) = c_0^2 \rho(x, y, z, t) = \Re\{\rho_0 i \omega \phi(x, y, z) e^{-i \omega t}\}, \quad (2)$$

where  $\rho_0$  is the ambient fluid density, and similarly the velocity fluctuations are

$$\mathbf{u}(x, y, z, t) = \Re\{\nabla \phi(x, y, z) e^{-i \omega t}\}. \quad (3)$$

For brevity we omit the exponential time-factor and real part braces until the end.

Omitting all details regarding the derivation of an effective boundary condition for a perforated elastic plate (instead referring the reader to the article by Leppington<sup>5</sup>), we state the equations for a structure consisting of two thin elastic plates, each of bending stiffness  $B$ , density  $\rho_p$  and thickness  $h$ , separated by a light but acoustically rigid honeycomb structure of width  $d$ . Round perforations of hole size  $2a$  are included on the top plate, and for the sake of mathematical simplicity, the honeycomb arrangement is taken so that each cavity is a cuboid with height  $d$ , and widths in the  $x$  and  $z$  directions of  $d_1$ , as shown in Fig. 1. Then, for  $kd \ll 1$ ,  $kd_1 \ll 1$ ,  $kh \ll 1$ ,  $ka \ll 1$  where  $k = \omega/c_0$ , we find that the composite plate structure satisfies (see, e.g., Ref. 11)

$$\left\{ 2B \left( \frac{\partial^2}{\partial x^2} + \frac{\partial^2}{\partial z^2} \right)^2 - 2\omega^2 \rho_p h \right\} \eta(x, z) - F(x, z) = i\omega \rho_0 \phi(x, 0^-, z) - i\omega \rho_0 \phi(x, 0^+, z) \quad (4)$$

on  $y=0$ , in which  $\eta(x, z)$  is the deflection of the plate in the  $y$  (vertical direction) and the right hand side is the pressure jump across the plate [i.e.,  $0^+$  ( $0^-$ ) indicates that  $y$  goes to zero from above (below)]. The function  $F(x, z)$  is the imposed plate forcing to be specified later. The vertical velocity of the plate must equal the fluid velocity on the plate's underside, but the holes on the top plate means that this is not so in general for the fluid velocity above. Hence,

$$\eta(x, z) = \frac{i}{\omega} \frac{\partial \phi}{\partial y}(x, 0^-, z), \quad (5)$$

and the pressure above the plate is related to the jump in velocity across the structure<sup>5</sup> via

$$\frac{\partial \phi}{\partial y}(x, 0^+, z) - \frac{\partial \phi}{\partial y}(x, 0^-, z) + k\tau \phi(x, 0^+, z) = 0 \quad (6)$$

in which the perforation parameter  $\tau$  is

$$\tau = 2fkda/[2a - k^2V], \quad (7)$$

$f$  is the fraction of cells with apertures,  $V$  is the volume of each cell and  $d, a$  are the plate spacing and perforation hole radius, respectively. For the cuboid cavities mentioned above, with a single hole in each one, we find

$$\tau = 2kda/[2a - k^2dd_1^2], \quad (8)$$

and note that the cavities resonate (Helmholtz resonance) when  $\tau \rightarrow \infty$ , or when

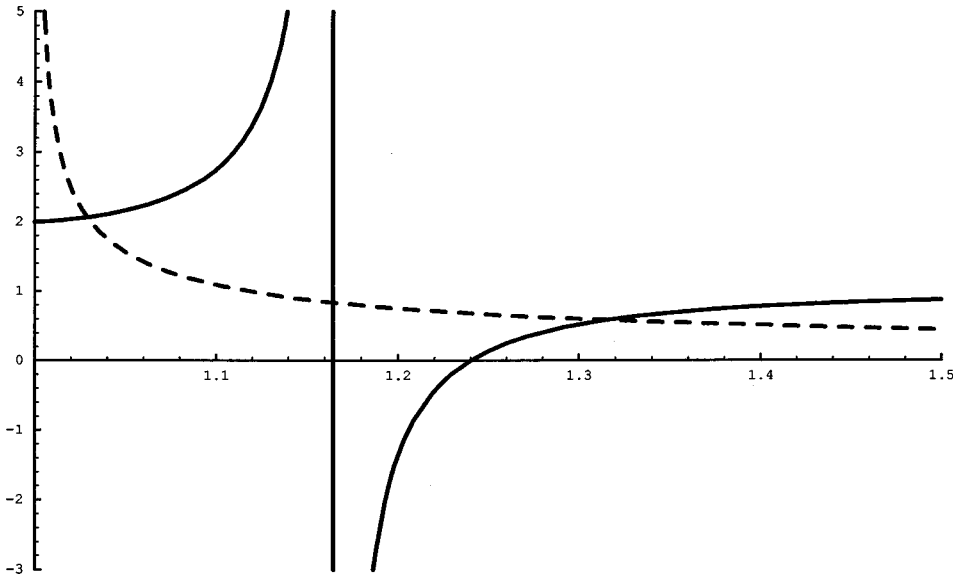


FIG. 2. Roots of the dispersion relation (23) given by the intersection of the function on the right (dashed line) and left (solid line) hand sides of (24).

$$k^2 = \frac{2a}{dd_1^2} \Rightarrow \omega = \sqrt{\frac{2a}{d} \frac{c_0}{d_1}}. \quad (9)$$

It is worth observing from (9) that the constraint

$$kd_1 \ll 1 \quad (10)$$

remains valid at or near a Helmholtz resonance if and only if

$$a \ll d. \quad (11)$$

Note that in the Leppington model used above the long-wavelength assumption allows the sandwich plate to be approximated by one of infinitesimal thickness [(4) and (6)]; by this means, all the details of the perforations and cell geometry are conveniently wrapped up in the single parameter  $\tau$ . As  $\tau \rightarrow 0$  then the perforation's influence vanishes and we recover the usual flexural thin-plate equation, across which the fluid velocity is continuous. As already stated, large  $\tau$  indicates that a Helmholtz resonance is approached, so that the perforations have a significant effect on the fluctuating field. Here we take  $\tau$  real, indicating that the flow in the cavity is lossless. However, if viscous motions through the apertures are assumed, then  $\tau$  will be complex, which will limit the maximum size of  $|\tau|$ . Other effects could also be included without difficulty, such as two or more different families of cavities, each yielding a different resonance value, i.e.,  $|\tau|$  will have multiple peaks when plotted over wave number.

As a final step in posing the problem, it is convenient to nondimensionalize using the acoustic wavelength and sound speed

$$(\bar{x}, \bar{y}, \bar{z}) = (kx, ky, kz), \quad \bar{\phi}_j = \frac{k}{c_0} \phi_j, \quad j = 1, 2, \quad (12)$$

where we write  $\phi_0$  ( $\phi_1$ ) as the acoustic potential below (above) the composite plate. Also, for the purposes of this article, we take a simple line force and bending moment acting upon the plate on  $\bar{x} = 0, \nabla \bar{z}$ . Thus, the forcing and plate geometry are independent of  $\bar{z}$  and so the boundary value problem may be considered as two-dimensional, the  $(\bar{x}, \bar{y})$ -plane. Summarizing, and dropping the overbars on the dimensionless variables for convenience, we have

$$\left( \frac{\partial^2}{\partial x^2} + \frac{\partial^2}{\partial y^2} + 1 \right) \phi_0(x, y) = 0, \quad y \leq 0, \quad -\infty < x < \infty, \quad (13)$$

$$\left( \frac{\partial^2}{\partial x^2} + \frac{\partial^2}{\partial y^2} + 1 \right) \phi_1(x, y) = 0, \quad y \geq 0, \quad -\infty < x < \infty, \quad (14)$$

and on the plate

$$\left( \frac{\partial^4}{\partial x^4} - \mu^4 \right) \frac{\partial \phi_0}{\partial y} + \alpha (\phi_1 - \phi_0) = A \delta(x) + B \delta'(x), \quad y = 0, \quad -\infty < x < \infty, \quad (15)$$

with the fluid velocity jump determined by

$$\frac{\partial \phi_1}{\partial y} - \frac{\partial \phi_0}{\partial y} + \tau \phi_1 = 0, \quad y = 0, \quad -\infty < x < \infty. \quad (16)$$

Here, the  $\mu$  and  $\alpha$  are

$$\mu^4 = \frac{\rho_p h c_0^4}{\omega^2 B}, \quad \alpha = \frac{\rho_0 c_0^5}{2 \omega^3 B}, \quad (17)$$

which, with  $\tau$  defined in (8), give three nondimensional fluid/structure coupling parameters for the problem. Note that  $\mu$  is the (dimensionless) wave number of free waves on the plate *in vacuo*. The first term on the right hand side of (15) is a line force of magnitude  $A$  and the second is a bending moment of strength  $B$  [ $\delta(x)$  is the usual generalized function and the dash denotes differentiation with respect to its argument]. These coefficients,  $A$  and  $B$ , can be chosen as desired. Equations (13)–(16), together with the condition of outgoing waves at infinity constitute the boundary value problem to be solved.

## II. UNATTENUATED PLATE WAVES

To examine free plate modes for the homogeneous coupled/plate system it is convenient to try the following form for a surface wave:

$$\phi_s = e^{isx - \gamma(s)|y|} \times \begin{cases} a, & y > 0, \\ b, & y < 0, \end{cases} \quad s \text{ real.} \quad (18)$$

Clearly (by direct substitution)  $\phi_s$  satisfies (13) and (14) if

$$\gamma^2(s) = s^2 - 1, \quad (19)$$

and so the wave will decay exponentially away from the plate if and only if

$$|s| > 1, \quad (20)$$

or  $\gamma(s) = (s^2 - 1)^{1/2} > 0$ . For  $|s| < 1$  then  $\gamma(s)$  is pure imaginary, and so (18) represents a plane wave which takes energy away from the plate. Hence, for study of surface waves in which the energy is constrained close to the plate the condition (20) is required. Substituting (18) into the homogeneous form of (15) yields

$$(s^4 - \mu^4)\gamma(s)b + \alpha(a - b) = 0 \quad (21)$$

and similarly (16) gives

$$-\gamma(s)(a + b) + \tau a = 0. \quad (22)$$

The two equations yield a nontrivial solution if and only if the determinant vanishes:

$$K(s) = [(s^4 - \mu^4)\gamma(s) - \alpha](\tau - \gamma(s)) + \alpha\gamma(s) = 0, \quad (23)$$

the left hand side of which is referred to as the dispersion relation for  $s$ . Rearranging gives an alternative form of constraint on  $s$ , namely

$$\frac{(s^4 - \mu^4)\gamma(s) - 2\alpha}{(s^4 - \mu^4)\gamma(s) - \alpha} = \frac{\tau}{\gamma(s)}. \quad (24)$$

The last expression is useful as it is simple to examine the limiting cases  $\tau \rightarrow 0$ ,  $\tau \rightarrow \infty$ . As  $\tau \rightarrow 0$  the equation reduces to

$$(s^4 - \mu^4)\gamma(s) - 2\alpha = 0, \quad (25)$$

whereas for  $\tau \rightarrow \infty$ ,

$$(s^4 - \mu^4)\gamma(s) - \alpha = 0, \quad (26)$$

which correspond to the usual thin-plate dispersion relations when the fluid is on both and one side, respectively (see, e.g., the article by Cannell<sup>12</sup>). This is as it should be; when  $\tau \rightarrow 0$  the perforations are closed yielding the usual plate equation, but as  $\tau \rightarrow \infty$  the perforation flow is large and so the effect of the fluid above the plate becomes negligible.

For all values of  $\mu$ ,  $\alpha$ , it is known that (25) and (26) each have one and only one positive real root (and one real negative root due to even behavior in  $s$ ) at  $s_2^*$ ,  $s_1^*$  say, respectively, where  $s_2^* > s_1^*$ . To see this, plot  $s^4 - \mu^4$  and  $c/\gamma(s)$ ,  $c > 0$ , against  $s$  for  $s \geq 1$ . As the first function is monotonic increasing with a finite value at  $s = 1$ , and the second is monotonic decreasing with value  $+\infty$  at  $s = 1$ , then there is clearly one unique point of intersection for arbitrary real values of  $\mu$  and  $c$  ( $> 0$ ). The full dispersion curve can now be examined by plotting the left hand side (unbroken curve) and right hand side (dashed curve) of (24) for  $s > 1$  in Fig. 2. Again, it is easy to prove that the form of the function on the left hand side is as shown for all values of  $\alpha$ ,  $\mu$  and the dashed curve is for a finite nonzero value of  $\tau$ . That is, there are two, and two only, points of intersection corre-

sponding to two roots  $s_1$ ,  $s_2$ , say, of the original dispersion equation (23). In fact, a little elementary calculus shows that the unbroken curve may, in  $|s| > 1$ , have a turning point at the location  $\sqrt{(2 + \sqrt{4 + 5\mu^4})/\sqrt{5}}$ , which is always to the left of the point of divergence in Fig. 2,  $s_1^*$ , but this does not alter the number of roots of (24). As  $\tau \rightarrow 0$  the dashed curve moves down, hence moving the intersection points (roots) to

$$\tau \rightarrow 0, \quad s_1 \rightarrow 1, \quad s_2 \rightarrow s_2^*. \quad (27)$$

As will be shown in the next section, when  $\tau = 0$  the root  $s_1 = 1$  in fact gives no contribution, hence recovering the single plate unattenuated mode for the case of no perforations. As  $\tau \rightarrow \infty$ , the dashed curve is pushed upwards, yielding roots at

$$\tau \rightarrow \infty, \quad s_1 \rightarrow s_1^*, \quad s_2 \sim \tau. \quad (28)$$

Again, it will be shown that the  $s_2$  plate wave term has vanishing coefficient as  $\tau \rightarrow \infty$ , hence recovering just the single unattenuated plate wave term,  $s_1^*$ .

It is to be stressed that for all values of  $\alpha$ ,  $\mu$ ,  $\tau$  the dispersion relation (24) yields two, and two only, positive real roots. One can be assigned to be a modified form of the unperforated plate wave number, but the other is entirely new and until now undiscovered. The purpose of the following sections is, for a typical boundary value problem, to see if the new plate wave term has a contribution to the sound field of the same order as the usual plate wave term (or perhaps larger) for typical values of fluid/plate parameters. If it has, then the effect of the perforations can be seen as significant on the scattered/radiated field in such models.

### III. SOLUTION OF THE BOUNDARY VALUE PROBLEM

To solve the system of equations (13)–(16) it is convenient to define the Fourier transform pair

$$F(s) = \int_{-\infty}^{\infty} f(x) e^{isx} dx, \quad (29)$$

$$f(x) = \frac{1}{2\pi} \int_{\mathcal{C}} F(s) e^{-isx} ds, \quad (30)$$

where  $\mathcal{C}$  is the contour running along the real line, from  $-\infty$  to  $+\infty$ , indented above any singularities on the negative half-line and below those occurring on the positive half-line (see Fig. 3). The reason for passing above (below) singularities on the left (right) hand part of the real line is that, for the given time dependence, wave terms will be recovered that are outward propagating and *not* incoming. The Fourier transform of the reduced wave equations (13) and (14) is

$$\frac{d^2 \Phi_j}{dy^2} (s, y) + (1 - s^2) \Phi_j(s, y) = 0, \quad j = 0, 1, \quad (31)$$

which has the bounded/outgoing solution

$$\Phi_0(s, y) = C(s) e^{\gamma(s)y}, \quad y \leq 0, \quad (32)$$

$$\Phi_1(s, y) = D(s) e^{-\gamma(s)y}, \quad y \geq 0, \quad (33)$$

with  $\gamma(s)$  as given by (19). Here  $\gamma(s)$  is made single valued by cutting the plane from  $s = 1$  to  $+\infty$  in the first quadrant

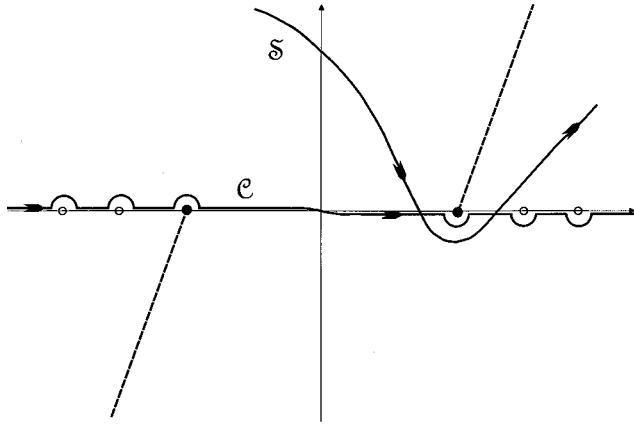


FIG. 3. The inverse transform path  $C$  of (30) passing above the branch point at  $-1$  and the simple poles at  $-s_1, -s_2$ , and below the branch point at  $+1$  and the poles at  $s_1, s_2$ . The branch cuts are denoted by dashed lines, and the steepest descent path for  $\theta > \pi/2$  is shown as  $S$ .

and  $s = -1$  to  $-\infty$  in the third quadrant, as shown by the dashed lines in Fig. 3, and choosing  $\gamma(0) = -i$ . Then  $\gamma(s)$  is negative imaginary for  $s$  real and  $|s| < 1$ , which implies that (32) and (33) are outgoing as  $y \rightarrow -\infty, +\infty$ , respectively, in view of the chosen time dependence (2). Also, for  $|s| > 1$  then  $\gamma(s) > 0$  and so  $\Phi_0$  and  $\Phi_1$  decay exponentially as  $y \rightarrow -\infty, +\infty$ , respectively.

The Fourier transform of the perforated plate equations (15) and (16) gives

$$(s^4 - \mu^4) \frac{d\Phi_0}{dy} + \alpha(\Phi_1 - \Phi_0) = A - isB, \quad (34)$$

$$\frac{d\Phi_1}{dy} - \frac{d\Phi_0}{dy} + \tau\Phi_1 = 0 \quad (35)$$

on  $y=0$ , which allows  $C(s)$  and  $D(s)$  to be determined by direct substitution of (32) and (33). This yields

$$\gamma(s)(s^4 - \mu^4)C(s) + \alpha(D(s) - C(s)) = A - isB, \quad (36)$$

$$-\gamma(s)(D(s) + C(s)) + \tau D(s) = 0, \quad (37)$$

or inverting gives

$$\begin{pmatrix} C(s) \\ D(s) \end{pmatrix} = \frac{1}{K(s)} \begin{pmatrix} \tau - \gamma(s) & -\alpha \\ \gamma(s) & \gamma(s)(s^4 - \mu^4) - \alpha \end{pmatrix} \times \begin{pmatrix} A - isB \\ 0 \end{pmatrix}, \quad (38)$$

where  $K(s)$  is the dispersion function written in (23). The solution to the problem is therefore given by the inverse transforms:

$$\begin{aligned} \phi_0(x, y) &= \frac{1}{2\pi} \int_C \frac{(\tau - \gamma(s))(A - isB)}{K(s)} e^{-isx + \gamma(s)y} ds, \\ y &\leq 0, \end{aligned} \quad (39)$$

$$\begin{aligned} \phi_1(x, y) &= \frac{1}{2\pi} \int_C \frac{\gamma(s)(A - isB)}{K(s)} e^{-isx - \gamma(s)y} ds, \\ y &\geq 0, \end{aligned} \quad (40)$$

in which  $C$  runs from  $-\infty$  to  $+\infty$  on the real line but passing above the branch point at  $-1$  and the simple poles at  $-s_1, -s_2$  [zeros of  $K(s)$ ], and below the branch point at  $+1$  and the poles at  $s_1, s_2$  (see Fig. 3).

The most useful information to extract from the inverse integral representations is the far-field cylindrical wave pattern and the amplitudes of the unattenuated surface waves. The former is obtained by determining the contribution from the integral at the saddle point (when  $r = x^2 + y^2 \rightarrow \infty$ ). To achieve this end we write

$$x = r \cos(\theta), \quad y = r \sin(\theta), \quad -\pi < \theta < \pi, \quad (41)$$

and introduce the transformation

$$s = -\cos(|\theta| + iu), \quad (42)$$

which maps  $s=0$  to the point  $u = i|\theta| - i\pi/2$ . Thus

$$\gamma(s) = -\sin(|\theta| + iu) \quad (43)$$

has the correct value ( $-i$ ) at the image point of  $s=0$ , and the exponents of the integrands in (39) and (40) become

$$-isx - \gamma(s)|y| = ircosh(u). \quad (44)$$

The saddle point occurs at

$$u = 0 \Leftrightarrow s = -\cos|\theta|, \quad (45)$$

which lies between the image of the branch points, and the path of steepest descent from this point is the curve given by

$$\Re\{\cosh(u)\} = 1. \quad (46)$$

The contour of integration  $C$  is deformed into the steepest descent path  $S$ , shown in Fig. 3 for  $|\theta| > \pi/2$ , which, in the  $u$ -plane, is the path starting at  $-i\pi/2 - \infty$  passing through the origin at an angle of  $\pi/4$  radians to the real line, and ending at  $+i\pi/2 + \infty$ . Then, by the usual arguments (see, e.g., p. 34 of the monograph by Noble<sup>13</sup>), as  $r \rightarrow \infty$ ,

$$\phi_0(r, \theta) \sim D(\theta) \frac{e^{ir + i\pi/4}}{\sqrt{2\pi r}}, \quad -\pi \leq \theta \leq 0, \quad (47)$$

$$\phi_1(r, \theta) \sim D(\theta) \frac{e^{ir + i\pi/4}}{\sqrt{2\pi r}}, \quad \pi \geq \theta \geq 0, \quad (48)$$

with

$$\begin{aligned} D(\theta) &= \frac{\sin(\theta)(A + iB \cos(\theta))}{K(-\cos(\theta))} \\ &\times \begin{cases} (-i\tau - \sin(\theta)), & -\pi \leq \theta \leq 0, \\ \sin(\theta), & \pi \geq \theta \geq 0. \end{cases} \end{aligned} \quad (49)$$

Note, when  $\tau=0$ , then the potential field is odd in  $y$ , i.e.,  $\phi_0(r, -\theta) = -\phi_1(r, \theta)$  as expected, and as  $\tau \rightarrow \infty$ ,  $\phi_1(r, \theta) = \mathcal{O}(1/\tau)$  and

$$\begin{aligned} \phi_0(r, \theta) &\sim \frac{-i \sin(\theta)(A + iB \cos(\theta))}{[i(\cos^4(\theta) - \mu^4) \sin(\theta) - \alpha]} \frac{e^{ir + i\pi/4}}{\sqrt{2\pi r}}, \\ \pi &\leq \theta \leq 0. \end{aligned} \quad (50)$$

In the deformation of (39) and (40) from  $C$  to the steepest descent path  $S$  the poles corresponding to the unattenuated surface waves are crossed for values of  $|\theta|$  sufficiently close

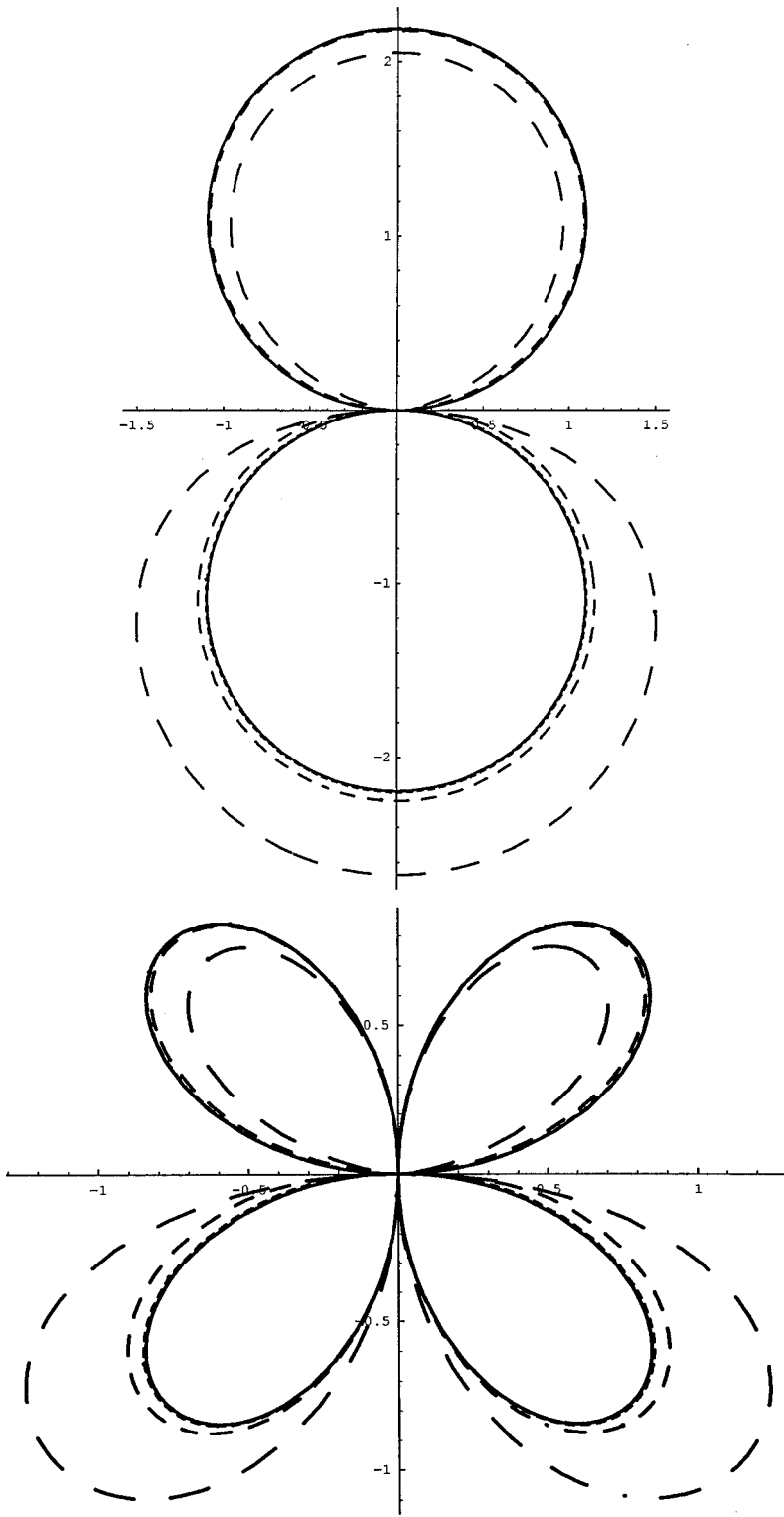


FIG. 4. Polar plots of the scaled amplitude of the far-field diffraction coefficient (49),  $|D(\theta)| \times 10^{15}/f^3$ , for an aluminum plate in water [parameter values as in (53)–(57)]. The curves are for frequencies 500 Hz (solid line), 1 KHz, 2 KHz, and 3 KHz (largest dash size), and forcing coefficients are (a)  $A=1, B=0$ , and (b)  $A=0, B=1$ .

to 0 or  $\pi$ . Picking up the residue contribution at these poles,  $s_1, s_2$ , gives

$$\phi_{s_j}(x, y) = \frac{i(A + is_j \operatorname{sgn}(x)B)}{K'(s_j)} e^{is_j x - \gamma(s_j)|y|} \times \begin{cases} \gamma(s_j), & y > 0, \\ \tau - \gamma(s_j), & y < 0, \end{cases} \quad (51)$$

for  $j=1,2$ , where  $s_j$  are the two positive real roots of  $K(s)$

$=0$ , (23),  $K'(s_j)$  is the derivative of  $K(s)$  evaluated at  $s_j$ , and, as expected, the applied force,  $A$ , and couple,  $B$ , yield even and odd behavior, respectively, in  $x$ . It will prove useful later to define the plate wave coefficient  $P_j$  as

$$P_j = \frac{i\gamma(s_j)(A + is_j \operatorname{sgn}(x)B)}{K'(s_j)}. \quad (52)$$

We can confirm directly from expression (51) that, as

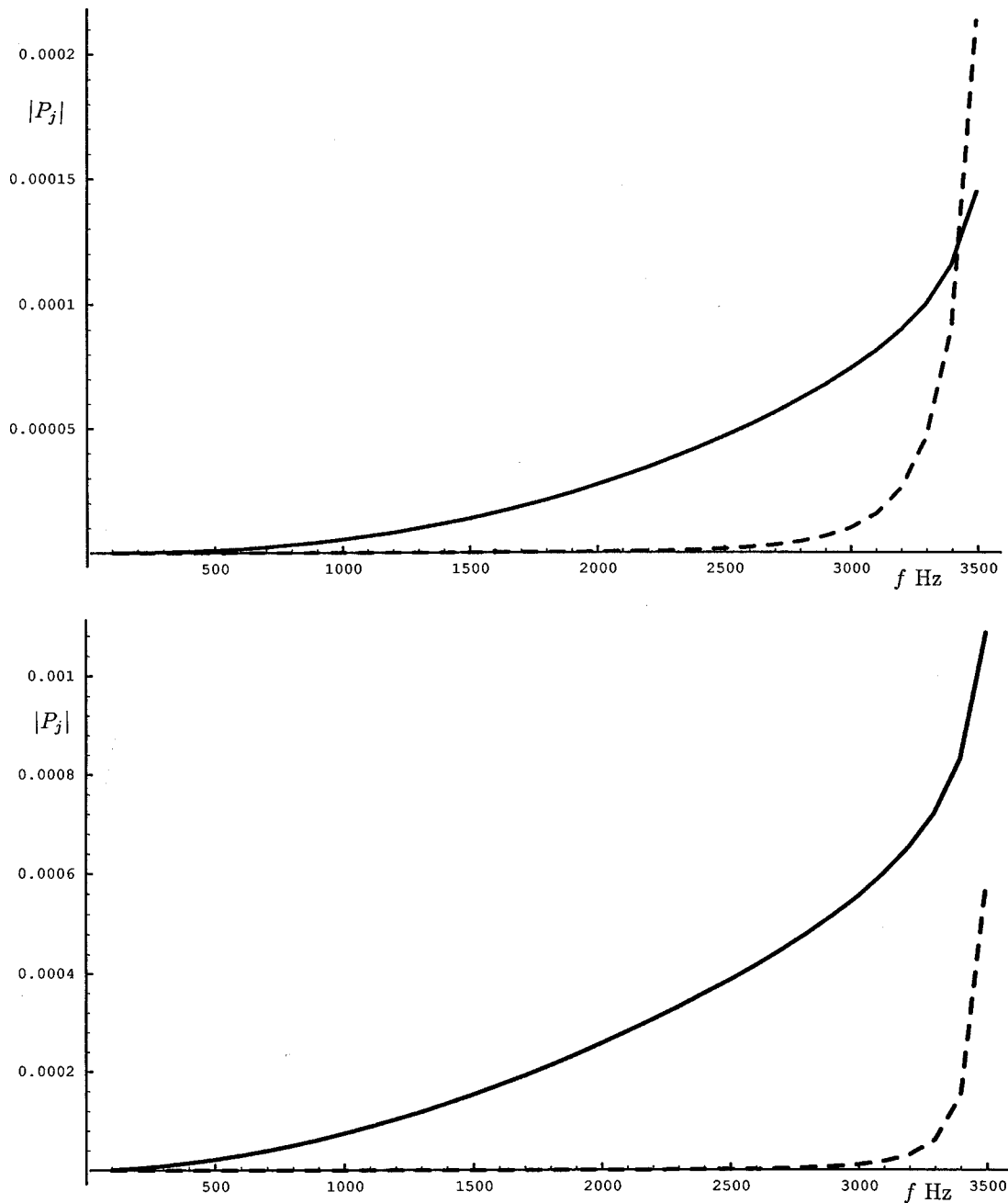


FIG. 5. Plate wave amplitudes (52)  $|P_1|$  (dashed line corresponding to root  $s_1$ ),  $|P_2|$  (solid curve for root  $s_2$ ) versus frequency,  $f$ , for an aluminum plate in water. Forcing coefficients are (a)  $A=1, B=0$ , and (b)  $A=0, B=1$ .

$\tau \rightarrow 0$ , the lower wave number root  $s_1$  (which tends to unity in this limit) has amplitude which goes to zero. Similarly, as  $\tau \rightarrow \infty$ , the upper root  $s_2 \sim \tau$ ,  $K'(s_2) \sim -\tau^5$ , and so  $\phi_{s_2} \rightarrow 0$ . Thus, in both limits only a single plate wave is recovered. This completes the solution of the boundary value problem, and in the following section we will numerically evaluate the far-field (47), (48) and plate wave terms (51) for a physically realistic range of values.

#### IV. NUMERICAL RESULTS AND CONCLUDING REMARKS

For brevity we will confine attention to a couple of sets of physically reasonable values for the nondimensional parameters. The composite plate will be taken to be made of

aluminum, with a thin acoustically rigid honeycomb spacer (of cuboid shape) in between; the values of the plate/cavity constants are

$$\rho_p = 2.8 \times 10^3 \text{ Kg/m}, \quad h = 2.5 \times 10^{-3} \text{ m}, \quad (53)$$

$$E = 7.4 \times 10^{10} \text{ N/m}^2,$$

$$\nu = 0.33, \quad d = 2 \times 10^{-2} \text{ m}, \quad d_1 = 2 \times 10^{-2} \text{ m} \quad (54)$$

(see Fig. 1), which are typical for normal engineering applications. Note that  $E$  and  $\nu$  are Young's modulus and Poisson's ratio, respectively, for the plate, from which we can deduce the bending stiffness:

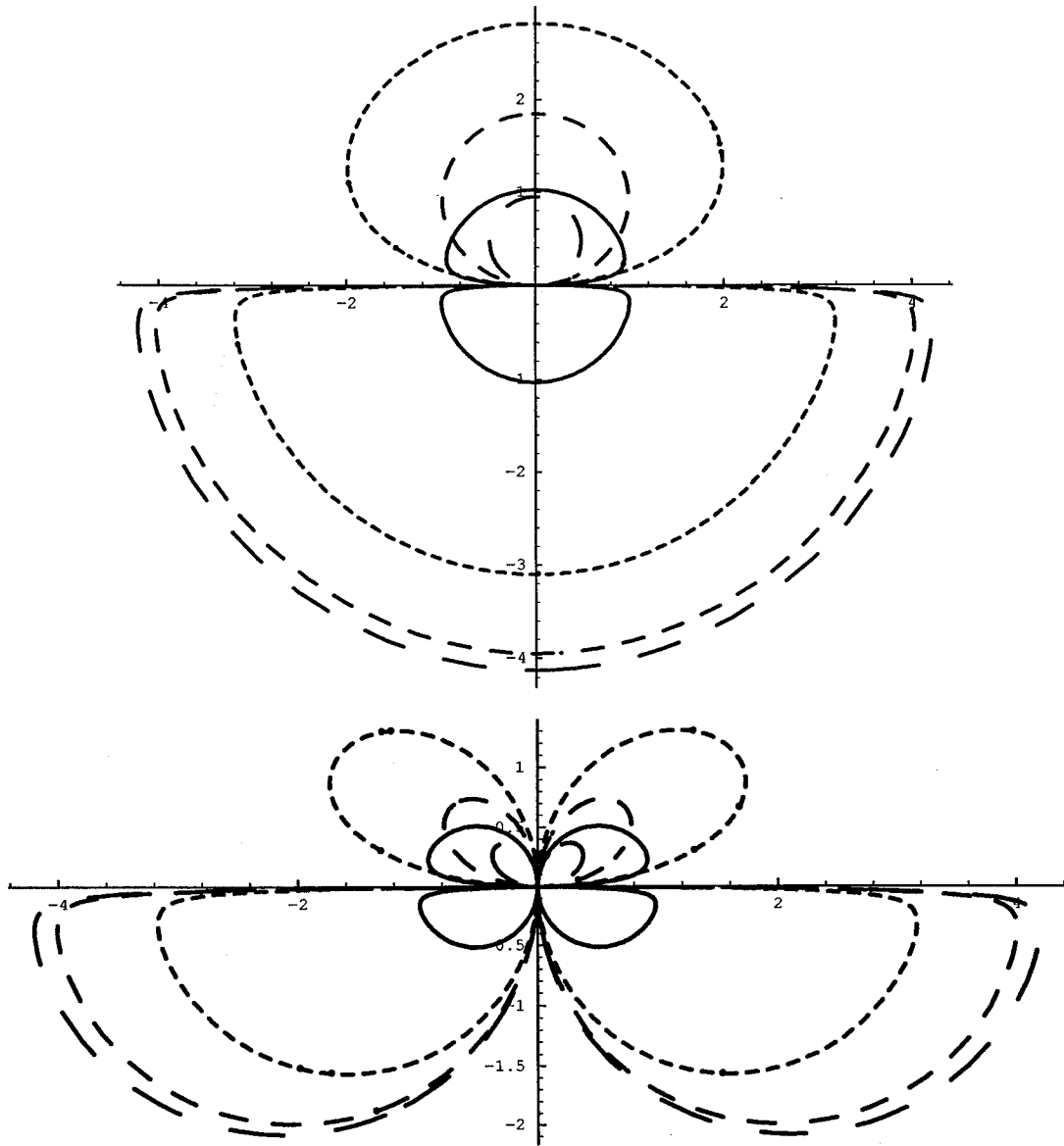


FIG. 6. Polar plots of the scaled amplitude of the far-field diffraction coefficient (49),  $|D(\theta)| \times 10^5 / f$ , for an aluminum plate in air [parameter values as in (53)–(56) and (59)]. The curves are for frequencies 200 (solid line), 600, 764, and 800 (largest dash size), and forcing coefficients are (a)  $A=1$ ,  $B=0$ , and (b)  $A=0$ ,  $B=1$ .

$$B = \frac{Eh^3}{12(1-\nu^2)} = 108.13 \text{ N m.} \quad (55)$$

Also, each cavity is assumed to have a single round perforation of radius

$$a = 1 \times 10^{-3} \text{ m.} \quad (56)$$

The embedding fluid is taken in the first instance as water, with density and sound speed

$$\rho_0 = 10^3 \text{ Kg/m}^3, \quad c_0 = 1439 \text{ m/s,} \quad (57)$$

and so

$$\mu \sim 289/f^{1/2}, \quad \alpha \sim 32717\mu^4/f, \quad \tau \sim \frac{3621f}{\sqrt{10(3621^2 - f^2)}} \quad (58)$$

in which  $f$  is the frequency of the forcing term. Note that we take  $f$  to lie below the Helmholtz frequency, 3621 Hz, in view of the assumptions used in Sec. I.

Figure 4(a) and (b) offer plots of the modulus of the far-field diffraction pattern,  $|D(\theta)|$ , over all  $\theta$  ( $-\pi < \theta < \pi$ ) for the aluminum plate in water and taking the loading, respectively, as a unit force,  $B=0$ ,  $A=1$ , and unit moment  $A=0$ ,  $B=1$ . Each polar plot gives four different values of forcing frequency,  $f=0.5, 1, 2, 3$  KHz (the corresponding  $\tau=0.0445, 0.0945, 0.251, 0.8354$ , respectively) and are marked in increasing dash size. The different curves are scaled using the factor  $10^{15}/f^3$  purely to allow them to be drawn on the same figure. As can be deduced from  $|D(\theta)|$ , the first field is dipole in form, whereas Fig. 4(b) exhibits quadrupole structure. The lobes in  $y > 0$  are roughly the same size as those in  $y < 0$ , i.e., the energy radiated above and below is more-or-less equal, except when the frequency ap-

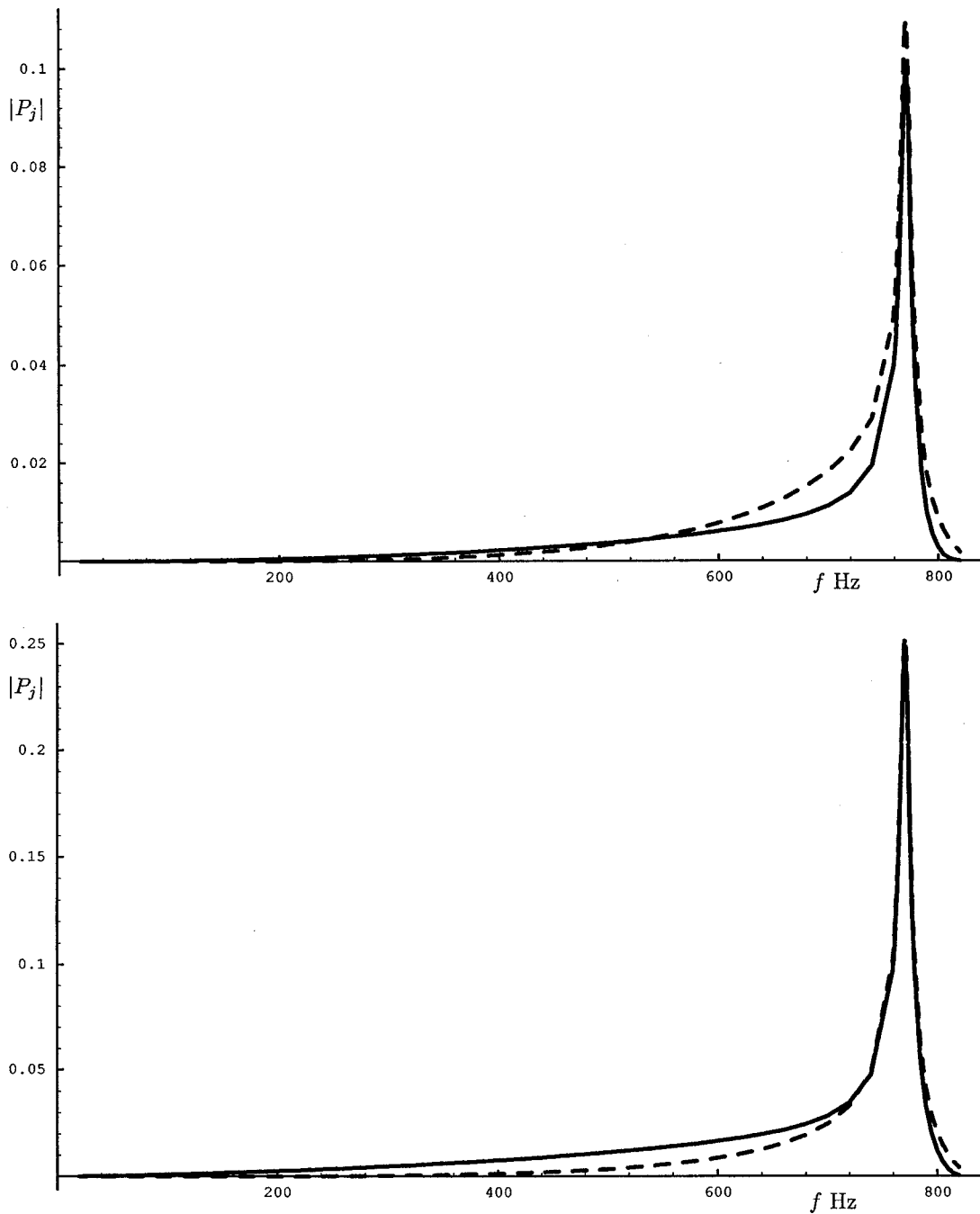


FIG. 7. Plate wave amplitudes (52)  $|P_1|$  (dashed line corresponding to root  $s_1$ ),  $|P_2|$  (solid curve for root  $s_2$ ) versus frequency,  $f$ , for an aluminum plate in air. Forcing coefficients are (a)  $A=1$ ,  $B=0$ , and (b)  $A=0$ ,  $B=1$ .

proaches the Helmholtz resonance value. Clearly the only significantly asymmetric curve is the one for  $f=3$  KHz. Related to Fig. 4 are the corresponding plate wave amplitude moduli  $|P_j|$  (52), where  $A=1$ ,  $B=0$  in Fig. 5(a),  $A=0$ ,  $B=1$  in Fig. 5(b), and  $j=1,2$  relates to the two plate wavenumbers  $s_1$ ,  $s_2$  ( $s_1 < s_2$ ) from (23). These figures strongly indicate the fact that the perforations are unimportant over most of the frequency range, that is,  $s_1$  has negligible amplitude in comparison with  $s_2$ , recognizable as the usual thin-plate wave component. So, the effect of the perforations on the radiated and plate wave fields only becomes important at frequencies very close to the Helmholtz resonance value.

The above figures could perhaps indicate the lack of

necessity for including a complicated perforated plate model except very close to the Helmholtz value. However, it is worth investigating the problem in a different physical situation, namely for an aluminum plate in air. Keeping plate/cavity values as those in (53)–(56), the fluid density and sound speed are now taken as

$$\rho_0 = 1.2 \text{ Kg/m}^3, \quad c_0 = 330 \text{ m/s}, \quad (59)$$

respectively. This gives the three dimensionless constants as

$$\mu \sim 66/f^{1/2}, \quad \alpha \sim 9\mu^4/f, \quad \tau \sim \frac{830f}{\sqrt{10(830^2 - f^2)}} \quad (60)$$

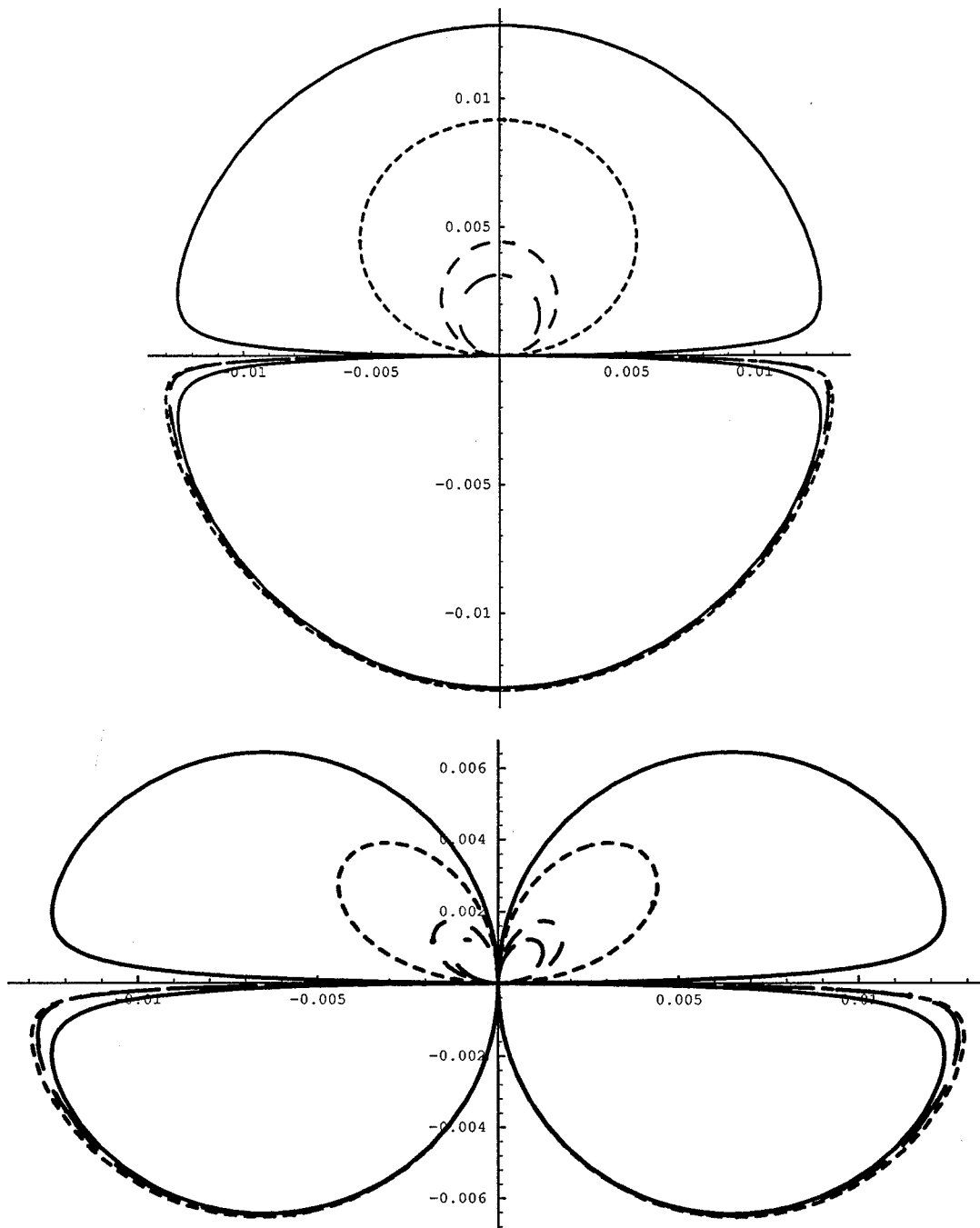


FIG. 8. Polar plots of  $|D(\theta)|$  (49) for an aluminum plate in air, with parameter values as in (53)–(56) and (59) and fixed frequency  $f=500$  Hz but with varying perforation parameter  $\tau$ . The curves are for values of  $\tau=0$  (solid line), 1, 2.75, and 4 (largest dash size), and forcing coefficients are (a)  $A=1$ ,  $B=0$ , and (b)  $A=0$ ,  $B=1$ .

in terms of the frequency  $f$ , and the structure has a Helmholtz resonance value of 830 Hz. The far-field amplitude plots,  $|D(\theta)|$ , for line force ( $B=0$ ) and moment ( $A=0$ ) are given in Fig. 6(a) and (b), for frequency  $f=200$  (continuous curve), 600, 764, and 800 Hz (largest dash size) (corresponding  $\tau$  values are 0.08, 0.48, 1.9, and 4.3, respectively). The amplitudes have again been scaled, this time by the factor  $10^5/f$ , in order to show the curves with approximately similar size in one figure. Notice that, despite the scaling factor decreasing with  $f$ , the curves increase in size in the region  $y < 0$ . However, there is a marked diminution in value of the ratio of energy flow above the plate as compared with radi-

ated energy below as the frequency increases. Not only can the cavity perforations be seen to be important in terms of the energy partitioning for frequencies above say 200 Hz, but in the line force case the remarkably uniform field (in  $\theta$ ) in  $y > 0$  is significantly modified as  $f$ , and hence  $\tau$  increases. This is to be contrasted with the field in  $y < 0$ , and Fig. 4(a) and (b) which do not exhibit any noticeable “beaming” effect. Most marked are the two noticeable lobes in  $y > 0$ , in Fig. 6(b), whose angle of radiation increases with frequency.

Turning now to the plate wave coefficients (52), these are computed for the parameter values (53)–(56) and (59) over the range of frequencies below resonance. As before, in

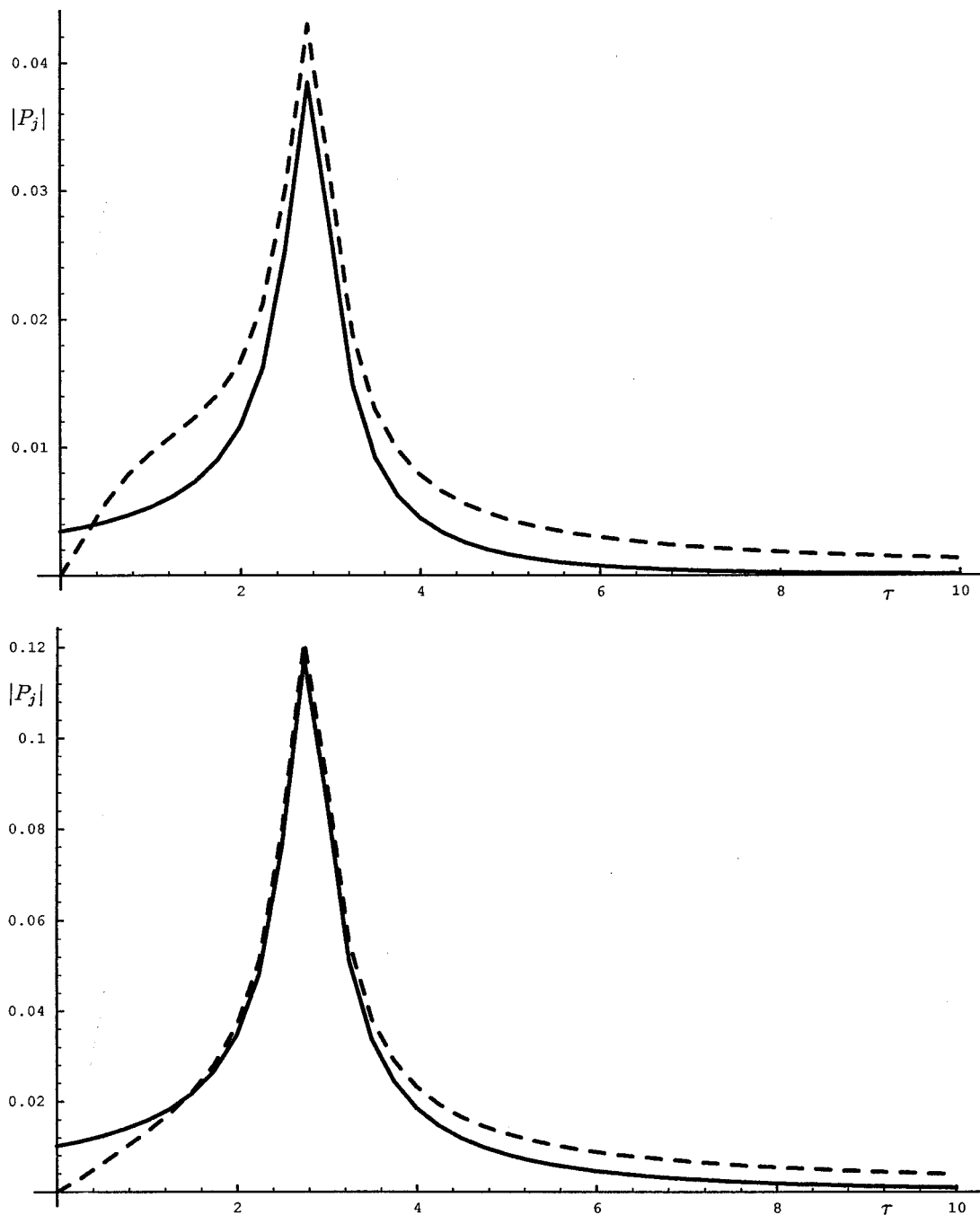


FIG. 9. Plate wave amplitudes (52)  $|P_1|$  (dashed line),  $|P_2|$  (solid curve) versus perforation parameter  $\tau$ , for an aluminum plate in air. Forcing coefficients are (a)  $A=1$ ,  $B=0$ , and (b)  $A=0$ ,  $B=1$ .

Fig. 7(a) and (b) the curve corresponding to the small wave number  $s_1$  is dashed, and the higher root,  $s_2$ , which becomes the usual propagating wave number as  $\tau \rightarrow 0$ , is the solid line. Immediately noticeable is the fact that, unlike the aluminum plate/water case [Fig. 5(a) and (b)], the coefficients take comparable values over most of the range of the ordinate. Therefore, energy partitioning has been affected by the modified plate model well away from the Helmholtz resonance value. Indeed, Fig. 7(a) shows that the new wave ( $s_1$ ) coefficient actually exceeds that of  $s_2$  at about 540 Hz (when  $\tau$  is just 0.357). However, the most significant, and unexpected, feature of graphs 7(a) and (b) is the presence of a very large peak at about 764 Hz [hence the reason for taking

this as one of the values in Fig. 6(a) and (b)]. This apparent “resonance” phenomenon does not seem to be easily attributable to any physical confluence of natural frequencies, etc. Nevertheless, at or very close to this value both wave modes attain very large (but finite) amplitudes, greater than 100 times larger than amplitudes at 200 Hz (corresponding to  $10^4$  times the energy in these surface waves)! Note that this is true for both traveling waves  $s_1$ ,  $s_2$ , and for arbitrary forcing (any values of  $A$ ,  $B$ ).

To illustrate the “pseudo-resonance” phenomenon a little more clearly, it is interesting to plot the radiated far-field and plate wave coefficients, at a fixed frequency, over a range of  $\tau$  values. This is tantamount to varying the cavities’

resonance parameters, such as by altering the perforation radius or cavity interior lengths. In Fig. 8(a) and (b),  $|D(\theta)|$  is plotted unscaled at a frequency of 500 Hz for four  $\tau$  values: 0 (solid line), 1, 2.75, 4 (largest dashed), and for the two cases of line force and moment loadings, respectively. Clearly, the radiated field into the region  $y < 0$  is remarkably insensitive to  $\tau$  values, whereas in  $y > 0$  there is a **monotonic decrease** in amplitude of the field with increasing  $\tau$ . Figure 9(a) and (b) show typical plate wave coefficients for the same frequency and forcing as in Fig. 8(a) and (b), respectively and with  $\tau$  varying from 0 to 10. As expected from the results of Sec. II [(27) and (28)], the coefficient of the  $s_1$  wave vanishes and  $s_2 \rightarrow s_2^*$  as  $\tau \rightarrow 0$ , and the coefficient of the  $s_2$  wave vanishes and  $s_1 \rightarrow s_1^*$  as  $\tau \rightarrow \infty$ . Clearly indicated is the fact that the amplitude of the  $s_2$  wave is only significantly greater than the  $s_1$  term for very small values of  $\tau$ . It can thus be concluded that for aluminum plates in air, perforated composite plate structures will have a significant effect on the radiation of sound into the enveloping fluid, even for modest  $\tau$  values. The very large amplitude of both plate waves at the “pseudo-resonance,” occurring in Fig. 9(a) and (b) at  $\tau = 2.775$ , is a totally unexpected feature, which may have important physical consequences. For example, there are significant structural dangers in employing finite panels with sharp resonance characteristics. Note, however, that nothing regarding a peak in the surface wave amplitudes at  $\tau \approx 2.75$  is apparently discernible from the cylindrical wave fields in Fig. 8(a) and (b).

In conclusion, this article has investigated the simple problem of sound radiation from an infinite perforated composite plate. It was shown that Leppington’s plate model<sup>5</sup> yields two distinct unattenuated surface waves for all non-zero values of the plate/fluid parameters. In the case of a sandwich construction for typical engineering applications, say composed of thin aluminum plates, the effect of perforations and an interior cavity was noticeable for problems in air but not so marked in underwater applications. In the former case, it is clear that **significant** modification to the energy radiation into the fluid above the plate (perforated side), and into the surface wave terms, occurs as  $\tau$  increases

from zero. An unexpected result is the discovery of a “resonant” frequency or  $\tau$  value at which both plate wave amplitudes increase dramatically. This is likely to be of significant engineering interest, if it proves not to be purely an artifact of the mathematical model, and is to be investigated further in a forthcoming article on the topic by the author.<sup>10</sup>

## ACKNOWLEDGMENTS

The author wishes to acknowledge useful discussions with Professor A. N. Norris, Rutgers University, and Professor F. G. Leppington, Imperial College, University of London, regarding the work contained in this article.

<sup>1</sup>F. Fahy, *Sound and Sources of Sound* (Academic, London, 1987).

<sup>2</sup>F. P. Grooteman and A. de Boer, “A symmetrical element formulation for sound transmission through fuselage walls; theory and application,” paper communicated to Euromech 369 Colloquium on *Fluid-Structure Interaction in Acoustics*, The Netherlands (1997).

<sup>3</sup>J. E. Ffowcs Williams, “The acoustics of turbulence near sound absorbent liners,” *J. Fluid Mech.* **51**, 737–749 (1972).

<sup>4</sup>F. G. Leppington and H. Levine, “Reflexion and transmission at a plane screen with periodically arranged circular or elliptical apertures,” *J. Fluid Mech.* **61**, 109–127 (1973).

<sup>5</sup>F. G. Leppington, “The effective boundary conditions for a perforated elastic sandwich panel in a compressible fluid,” *Proc. R. Soc. London, Ser. A* **427**, 385–399 (1990).

<sup>6</sup>C. M. A. Jones, “Scattering by a semi-infinite sandwich panel perforated on one side,” *Proc. R. Soc. London, Ser. A* **431**, 465–479 (1990).

<sup>7</sup>I. D. Abrahams, “Radiation and scattering of waves on an elastic half-space; a noncommutative matrix Wiener-Hopf problem,” *J. Mech. Phys. Solids* **44**, 2125–2154 (1996).

<sup>8</sup>I. D. Abrahams, “On the solution of Wiener-Hopf problems involving non-commutative matrix kernel decompositions,” *SIAM (Soc. Ind. Appl. Math.) J. Appl. Math.* **57**, 541–567 (1997).

<sup>9</sup>I. D. Abrahams, “On the non-commutative factorization of Wiener-Hopf kernels of Khrapkov type,” *Proc. R. Soc. London, Ser. A* **454**, 1719–1743 (1998).

<sup>10</sup>I. D. Abrahams, “Diffraction of sound by a semi-infinite sandwich panel,” *Proc. R. Soc. London* (submitted).

<sup>11</sup>M. C. Junger and D. Feit, *Sound, Structures and Their Interaction* (MIT, Cambridge, MA, 1986).

<sup>12</sup>P. A. Cannell, “Acoustic edge scattering by a heavily loaded elastic half-plane,” *Proc. R. Soc. London, Ser. A* **350**, 71–89 (1976).

<sup>13</sup>B. Noble, *The Wiener-Hopf Technique* (Chelsea, New York, 1988), 2nd ed.